# Field Manipulation of Band Properties in Infrared Spectra of Thin Films

(article starts on next page)

RESEARCH ARTICLE

**ADVANCED**
PHOTONICS
**RESEARCH**
Open Access

www.adpr-journal.com

# Field Manipulation of Band Properties in Infrared Spectra of Thin Films

*Karsten Hinrichs,\* Naveen Shetty, Sergey Kubatkin, Per Malmberg, Samuel Lara-Avila, Andreas Furchner, and Jörg Rappich*

This comprehensive optical study analyzes field manipulations of bands in infrared (IR) spectra of thin films and functional surfaces for varying measurement and sample conditions. Band variations related to the materials dielectric functions, the measurement geometry, the film thickness as well as the direction dependence of the probing electromagnetic fields are demonstrated. Examples are discussed for isotropic polymer films ($\approx$200 nm polymethylmethacrylate [PMMA]) on gold and silicon as well as an anisotropic hydrogen monolayer on a Si(111) surface, characterized by IR–attenuated total reflection, IR microscopy, and incidence-angle-dependent IR polarimetry. Even for fixed optical material properties, significant manipulations of band frequency and shape (shifts up to $\approx$14 cm$^{-1}$ for PMMA, up to $\approx$3 cm$^{-1}$ for H–Si) occur in not only polarization-dependent but also unpolarized spectra. The shown data underline that polarimetric measurements and optical analyses are essential for a detailed interpretation of band shapes.

K. Hinrichs
Department Application Labs Berlin
Leibniz-Institut für Analytische Wissenschaften – ISAS – e.V.
Schwarzschildstraße 8, 12489 Berlin, Germany
E-mail: karsten.hinrichs@isas.de

N. Shetty, S. Kubatkin, S. Lara-Avila
Department of Microtechnology and Nanoscience
Quantum Device Physics Lab
Chalmers University of Technology
Kemivägen 9, 41296 Gothenburg, Sweden

P. Malmberg
Department of Chemistry and Chemical Engineering
Chalmers University of Technology
41296 Gothenburg, Sweden

S. Lara-Avila
National Physical Laboratory
Hampton Road, Teddington TW11 0LW, United Kingdom

A. Furchner, J. Rappich
Young Investigator Group Nanoscale Solid–Liquid Interfaces
Helmholtz-Zentrum Berlin für Materialien und Energie GmbH
Schwarzschildstraße 8, 12489 Berlin, Germany

## 1. Introduction

Thin film materials are essential in a wide field of applications such as sensing,[1–4] separation,[2,5,6] optoelectronics,[1,4,7] energy,[1,5,8,9] transistors[3,10,11] polymer science,[1,12,13] material research, corrosion science,[1] environmental science[6] catalysis,[2,14,15] and biomedicine.[16–18] The specific infrared (IR) spectroscopic method to study these films must be chosen depending on the properties to be determined as well as the kind of sample, the specific material, and the environmental conditions. Among these methods are IR microscopy,[19,20] photothermal[21–25] or near-field scattering IR techniques,[26,27] 2D IR,[28,29] attenuated total reflection (ATR),[20,30] IR transmission,[20,31,32] external IR reflection,[20,31] or ellipsometric/polarimetric IR techniques.[13,33–39] Common for all methods is that the measured IR spectra are analyzed with respect to the apparent bands, which are often related to vibrational contributions.

In this work, far-field, microscopic and ATR techniques in reflection geometries are utilized. A sketch of a typical measurement geometry for reflection measurements at an incidence angle $\varphi_i$ is displayed in **Figure 1**. For polarimetric measurements, a polarizer is placed in the incident beam (subscript i) and an analyzer in the reflected beam (subscript r), enabling s- and p-polarized reflection measurements (s: polarization perpendicular and p: polarization parallel to the incidence plane) as well as ellipsometric measurements. A detector measures the reflected intensities ($I_{i,r}=|E_{i,r}|^2$) at a specific parallel polarizer/analyzer setting. Intensities of the incidence beam are measured in an empty channel in transmission (no sample) or by reflection using a known gold reference sample. The ellipsometric parameters are determined from intensity measurements at 0°, 45°, 90°, and 135° polarizer azimuths[33] and are defined by the quantity $\rho$,[38] which is the ratio of the complex reflection coefficients $r_p$ and $r_s$

$$\rho = \frac{r_p}{r_s} = \tan\Psi \, e^{i\Delta} \tag{1}$$

For refractive indices $n_1$ (ambient) $> n_2$ (film), ATR measurements are performed. More details on the typical measurement sizes discussed in this work are given in the inset on the right in Figure 1.

Each IR technique delivers specific spectral measurement variables, which can be interpreted by simulations[13,31,39,40–42] in

**Figure 1.** Sketch of measurement geometry for reflection measurements at an incidence angle $\varphi_i$ at a layered sample with refractive indices $n_1$ (ambient), $n_2$ (layer), and $n_3$ (substrate), $n_1 < n_2$ for far-field measurements, and $n_1 > n_2$ for ATR measurements. Some typical measurement variables are shown in the inset on the right.

optical layer models using an adequate description for the material optical functions. Numerical calculations based on solving Maxwell's equations at defined conditions such as finite element methods, finite-difference time-domain method, or rigorous coupled-wave analysis (limited to periodic systems) can support the analysis of measured IR spectra.[41] A well-known analytical interpretation of IR reflection (and transmission) is based on wave propagation equations in a $4 \times 4$ transfer matrix formulation.[43,44] This approach can be adopted to describe the reflection or the transmission of arbitrarily anisotropic and homogeneous layered systems.[45,46] Special solutions can be used for selected isotropic and anisotropic layers.[39,46] In the presented work, SpectraRay/4 (Sentech Instruments GmbH, Germany) was used for optical simulations based on the general $4 \times 4$ matrix formalism.

In the optical modeling, the vibrational contributions can be included by oscillator models (e.g., by harmonic/Lorentzian[33,42] or Voigt oscillators[47]). A best-fit simulation optimizing the difference between measured and simulated spectra serves to determine the respective material properties and geometrical properties (such as thicknesses or structural properties). Another result of the optical simulation is the material's inherent optical properties such as the complex refractive index $\tilde{n} = n_r + ik$ or the complex dielectric function $\tilde{\varepsilon} = \varepsilon_1 + i\varepsilon_2$, with $\varepsilon_1 = n^2 - k^2$ and $\varepsilon_2 = 2nk$.

These complex optical functions are often depending on ordering, morphology, composition, intra- and intermolecular interactions, and anisotropy.[13] For anisotropic and layered samples, optical simulations are essential to determine these optical functions. Only in a limiting case such as a bulk sample with neglectable surface properties, the measured ellipsometric parameters can be interpreted directly[42]

$$\langle \tilde{n} \rangle = \langle \tilde{\varepsilon} \rangle^{0.5} = \left( \sin^2(\varphi) \left[ 1 + \left( \frac{1-\rho}{1+\rho} \right)^2 \tan^2(\varphi) \right] \right)^{0.5} \quad (2)$$

As an example for such a case, an isotropic acrylic-glass bulk sample has been studied. The spectral pseudoabsorption index $k$

of acryl glass (polymethylmethacrylate, PMMA) determined from an IR ellipsometric measurement using Equation (2) is shown in **Figure 2**. General band assignments are also given. Some of the bands are related to multiple vibrational contributions, which, in turn, belong to complex displacement patterns involving different molecular parts. For a detailed discussion of vibrational assignments, we refer to Ref. [48].

The displayed absorption index $k$ in Figure 2 is a material-characteristic spectral fingerprint of the studied acryl glass. If other acryl glass samples with different material properties such as density, chemical structure, or tensions would be characterized, differences of the respective absorption indices would be visible to the eye. Such visual inspections are often sufficient to give a first answer to a specific analytical question. However, such a procedure could lead to misinterpretations of
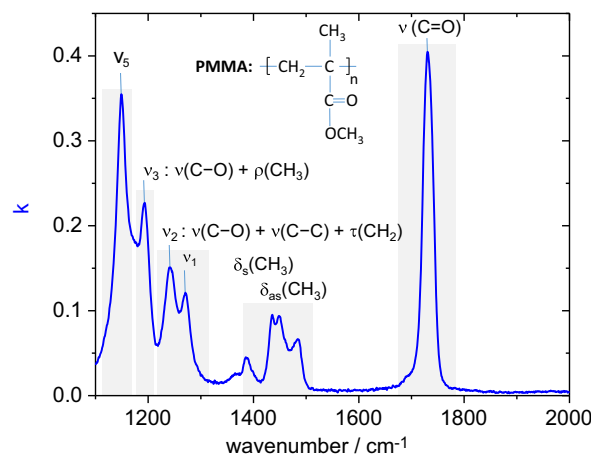


**Figure 2.** Absorption index $k$ of acryl glass determined ellipsometrically using Equation (2). Some characteristic bands are assigned to stretching ($\nu$), in-plane bending ($\delta$), rocking ($\rho$), and twisting ($\tau$) vibrations of the polymer according to ref. [48].

IR spectra depending on the thin film properties, the chosen incidence angle and polarization as well as the type of substrate (semiconducting, insulating, or metallic).

In the following, we study the influence of the substrate (metallic or semiconducting) as well as the incidence angle on the measured IR spectra. Discrepancies between the observed band properties in the absorption index and the imaginary part of the dielectric function are discussed. Hydrogen-passivated silicon surfaces as well as acrylic glass, PMMA layers on silicon, and gold are investigated in case studies.

Hydrogen passivation of amorphous and crystalline silicon bulk, films, and surfaces[49–58] is technologically highly relevant for the fabrication of integrated, sensing,[51] and solar cell devices.[54–56] Examples for IR spectroscopic investigations of hydrogen-passivated samples are identification and analysis of the formation of $Si–H_x$ groups,[50,53,57] the study of the ideality of the formed passivated interface,[57] the verification of the removal or formation of an interfacial oxide layer,[58] and the analysis of a subsequent functionalization.[52]

PMMA is a popular resist in microfabrication processes involving electron beam, photo-, and soft lithography.[59–63] As such, the technology to prepare high-quality thin films of PMMA by, e.g., spin coating is well established. Moreover, PMMA thin films are highly relevant for a wide range of applications,[64] including sensing,[65,66] optical/photonic devices,[67,68] and microfluidic systems,[69] to mention a few. More recently, PMMA has been instrumental to enable the transfer, passivation, and functionalization of 2D materials.[70–73] For the latter, PMMA has been shown to allow the diffusion of molecular dopants and enable the spontaneous assembly of molecular layers on graphene, with optimal results for a 200 nm thick PMMA layer prepared by spin coating and baking at $T = 170\,°C$.[73] In the literature, IR spectroscopy has been shown to be a useful tool for PMMA analysis of vibrational,[48,74] conformational order,[75,76] rheological,[75] and optical properties.[77]

Here, typical IR techniques available in many labs are discussed for the study of PMMA: ATR and IR microscopy at low incidence angles. To understand the unpolarized measurements with these two techniques, additional analytical optical simulations and polarization-dependent measurements are performed. Afterward, a detailed discussion of polarimetric spectra at higher incidence angles is given.

## 2. Results

### 2.1. Isotropic PMMA Bulk and Layer Samples: ATR and IR Microscopy

An ATR spectrum of acryl glass is investigated as a first example. **Figure 3** shows the previously introduced absorption index $k$ (blue) from ellipsometry measurements in comparison to the measured ATR absorbance spectrum (red) of the same material. Although the spectral signatures in the $k$ and ATR spectra look quite similar, there are obvious deviations. These differences could originate from the fact that ATR measurements only probe the top few µm of the acryl glass in a contact measurement, whereas ellipsometry probes a much larger volume of the sample in a noncontact fashion to determine $k$ according to Equation (2).

Significant differences between the spectra are observed for the two regions of strong vibrational absorption below $1200\,cm^{-1}$ and around $1730\,cm^{-1}$. In both regions, the frequency of the respective bands is significantly shifted between the absorption spectrum $k$ and the ATR absorbance reflection spectrum. To display this shift more clearly, a zoom for the region around $1730\,cm^{-1}$ is presented on the right of Figure 3. Despite the apparent shift, a calculated ATR spectrum (black dashed line), computed by the shown $k$ data, does in fact reproduce the frequency of the band in the ATR spectrum. In other words, a direct reading of the band frequency from a
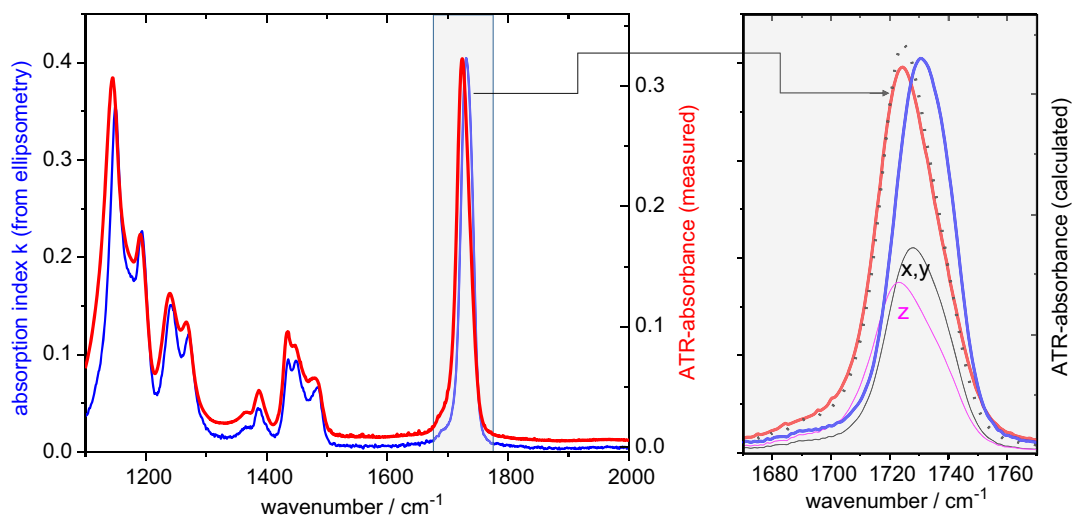


**Figure 3.** Left: Ellipsometrically determined absorption index $k$ of acryl glass (blue) in comparison to the measured ATR absorbance $[-\log(I/I_0)]$ (red) acquired with a 36× Ge objective in a BRUKER Hyperion 3000 IR microscope at defined pressure level and controlled focus position with a photovoltaic mercury cadmium telluride (MCT) detector[34] at $1\,cm^{-1}$ spectral resolution ($\varphi_i = 30 \pm 5.05°$). Right: Zoom into the C=O frequency region, with calculations for solely in-plane (x,y: black thin line) and out-of-plane (z: magenta thin line) components. A calculated ATR absorbance spectrum based on the $k$ spectrum (black dotted line) is also shown.

**ADVANCED
SCIENCE NEWS**

www.advancedsciencenews.com

**ADVANCED
PHOTONICS
RESEARCH**
Open Access

www.adpr-journal.com

measured ATR spectrum could mistakenly yield a different (wrong) frequency than the one seen in the absorption index of the same material. Therefore, a direct reading of the band could also lead to false conclusions on the material properties of the sample.

Note that, although the studied material is isotropic, the bands related to absorptions produced by its in-plane and out-of-plane components of the same vibrational contribution are not identical. To illustrate this point, calculated ATR spectra with solely in-plane ($x,y$: black thin line) and solely out-of-plane components ($z$: magenta thin line) are also shown in Figure 3 (right).

For reflection experiments outside the range of optical total reflection, the situation could be even more complex because the vibrational bands observed in such reflection spectra are more strongly modulated by a varying refractive index responsible for a spectrally varying transmission/reflection at the layer surface/interface. Exemplarily, a 194 nm (193.84 ± 0.02 nm) thick PMMA layer on an Au substrate was studied. The experimentally determined dielectric function of PMMA on Au served for the further analytical optical interpretations. Details on evaluation in a best-fit simulation are given in Supporting Information.

The PMMA film was then measured with IR microscopy. **Figure 4** compares (a) an unpolarized reflection spectrum R with (b) the corresponding absorption index $k$ and the (scaled) imaginary part of the dielectric function $\varepsilon_2$, as well as (c) s-

and p-polarized reflection spectra $R_s$ and $R_p$. The used IR microscope's Cassegrain objective has a rather low average incidence angle (about 17°). The presented types of spectra exhibit marked differences. Above 1735 cm$^{-1}$, the band shape in R deviates from the one in $k$ and $\varepsilon_2$ (Figure 4b). Comparing R with a scaled "$1 - k$" spectrum (black in Figure 4a) makes this deviation more apparent. The direction-dependent contributions in the whole band become clearer in the polarization-dependent reflection spectra, as indicated by a blue (in–plane contribution) and a magenta (out-of-plane contribution) arrow (Figure 4c). The shape of $\varepsilon_2$ reflects very well the one of $R_s$, as can be seen by the thin gray line in Figure 4c representing a scaled "$1-\varepsilon_2$" spectrum. On the other hand, $R_p$ (magenta) shows a broadband that deviates in shape from the one of both $\varepsilon_2$ and $k$ (imaginary parts of the optical functions). Qualitatively, this broad band in $R_p$ can be understood by two spectrally differing absorptions related to in-plane (separately observed in s-polarized reflection) (blue arrow) and to out-of-plane (magenta arrow) directed absorptions.

In summary, the seemingly simple analytical problem to characterize an isotropic bulk and an isotropic thin polymer film sample with IR–ATR and IR microscopy shows how complex the interpretation of band shapes and band frequencies can be. In fact, analytical calculations are required to understand the measured spectra quantitatively. Spectral comparisons with optical functions and polarization-dependent studies support the understanding of observed band shapes in unpolarized IR–ATR- and IR-microscopic spectra. For oscillators with high absorption, a direct read-out of band frequencies from measured spectra is not possible. The band shape in unpolarized reflection spectra can be understood by considering different band contributions for the same vibrational resonance in s- and p-polarized spectra.
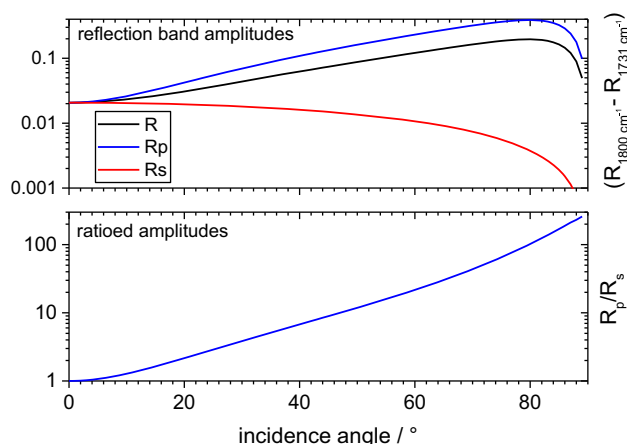
In the following sections, these effects are investigated in more detail. Thin isotropic polymer layers on a metallic and a semiconducting substrate are analyzed with polarimetric measurements at varying incidence angles.

## 2.2. Isotropic PMMA Layer on a Gold Substrate: Angle- and Polarization-Dependent Reflection Spectroscopy

**Figure 5** shows the calculated incidence-angle-dependent behavior of unpolarized (R), p-polarized ($R_p$), and s-polarized ($R_s$) band amplitudes at 1731 cm$^{-1}$ of the 194 nm thick PMMA layer on gold, as well as the ratio of $R_p/R_s$. At a low incidence angle, the p- and the s-polarized contributions are of similar amplitude (as also previously observed in Figure 4c at about 17° incidence angle). For higher incidence angles, the so-called "surface selection rule"[78] dominates; the in-plane directed electric field is screened, causing the suppression (although not perfect) of the in-plane directed absorption for the PMMA layer on Au.

Results of a detailed incidence-angle-dependent spectral study of the 194 nm polymer layer are presented in **Figure 6**. Normalized measured (a) and calculated (b) angle-dependent negative $R_p$ and $R_s$ spectra are shown. Excellent agreement between measurement and calculation is found. Obviously, the band shape depends on the incidence angle for the p-polarized experiment, but it does not vary for s-polarized reflection. This behavior can be understood by the fact that electromagnetic fields in direction of the surface normal exist only for the



**Figure 4.** a) IR-microscopic unpolarized reflection R (green) and scaled "$1 - k$" spectrum (thin black line) of a 194 nm thick PMMA layer on gold. b) Absorption index $k$ (red) and scaled imaginary part of the dielectric function $\varepsilon_2$ (blue). c) s (magenta) and p-polarized (blue) IR-microscopic reflection spectra $R_s$ and $R_p$, and scaled "$1-\varepsilon_2$" spectrum (thin black line). A 15× Cassegrain objective with an average incidence angle of 17° was used at 1 cm$^{-1}$ spectral resolution.

**ADVANCED
SCIENCE NEWS**

www.advancedsciencenews.com

**ADVANCED
PHOTONICS
RESEARCH**
Open Access

www.adpr-journal.com

**Figure 5.** Calculated incidence-angle-dependent unpolarized ($R$), p-polarized ($R_p$), and s-polarized ($R_s$) band amplitudes ($R_{1800\,cm^{-1}} - R_{1731\,cm^{-1}}$) of a 194 nm thick PMMA layer on gold, and the ratio $R_p/R_s$.

p-polarized measurements. These fields can manipulate the absorption in dependence of their strengths and the strengths of the probed oscillator.[7,79–82] Therefore, the frequencies of the band maximum increase stronger toward higher incidence angles for the p-polarized spectra. The band shape in the s-polarized spectra resembles the one in $\varepsilon_2$.

In summary, strong variations of band shape and band frequency are identified in the measured p-polarized spectra in dependence of the incidence angle. It is difficult, if not
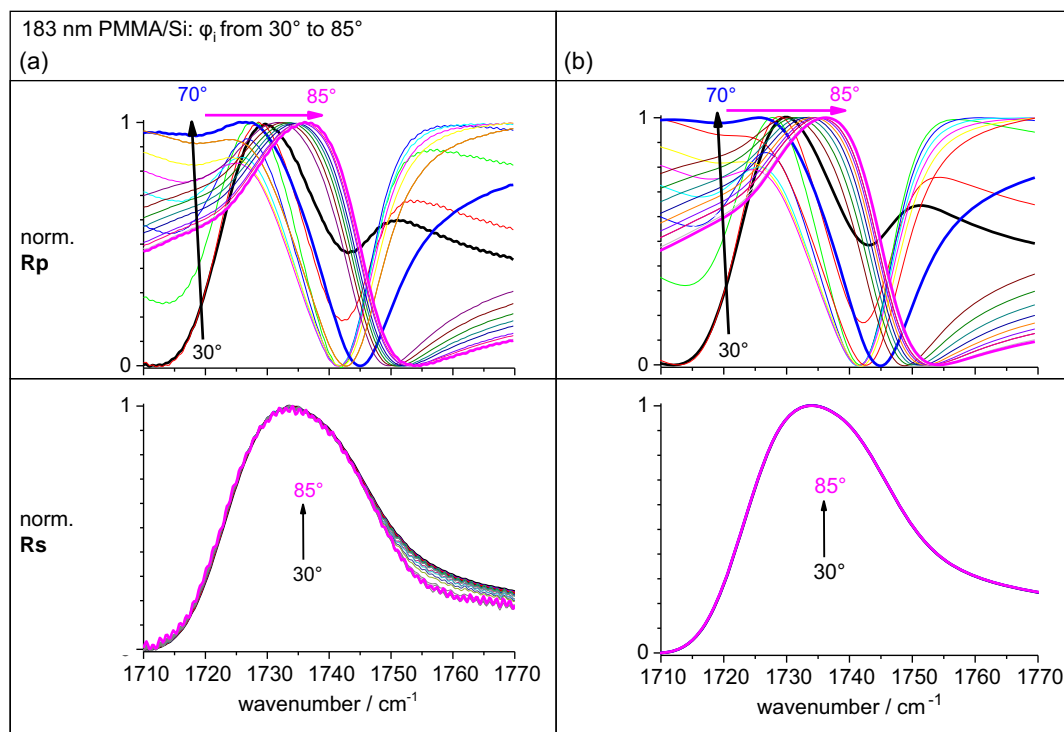
impossible, to identify resonance frequencies directly in the measured spectra (in agreement with the results of the previous section on microscopic and ATR spectra) and that the observed band shapes in the p-polarized spectra are deviating from those observed in the material optical functions. Only for the s-polarized spectra, the band shape resembles the one of $\varepsilon_2$. This suggests that in the general case, even for an isotropic thin film, an analytical optical interpretation of IR spectra is required for quantitative considerations.

## 2.3. Isotropic PMMA Layer on a Silicon Substrate: Angle- and Polarization-Dependent Reflection Spectroscopy

Similar to the PMMA layer on gold discussed previously, **Figure 7** shows normalized measured (a) and calculated (b) $R_p$ and $R_s$ spectra of a 183 nm thick PMMA layer on silicon. Again, good agreement is found between measurement and calculation (based on the same optical constants as used for the layer on gold, see Supporting Information). Pronounced variations in the spectra are observed with changes in incidence angles. The band shape in $R_p$ varies significantly, which makes it impossible to identify by eye bands that resemble those from vibrational resonances in the material optical functions. Different trends for the spectral variations are observed below and above the Brewster angle (indicated by arrows). The band shape is almost constant only for the s-polarized spectra (only in-plane-related absorptions). However, for lower incidence angles, some disturbances such as a slight baseline shift and
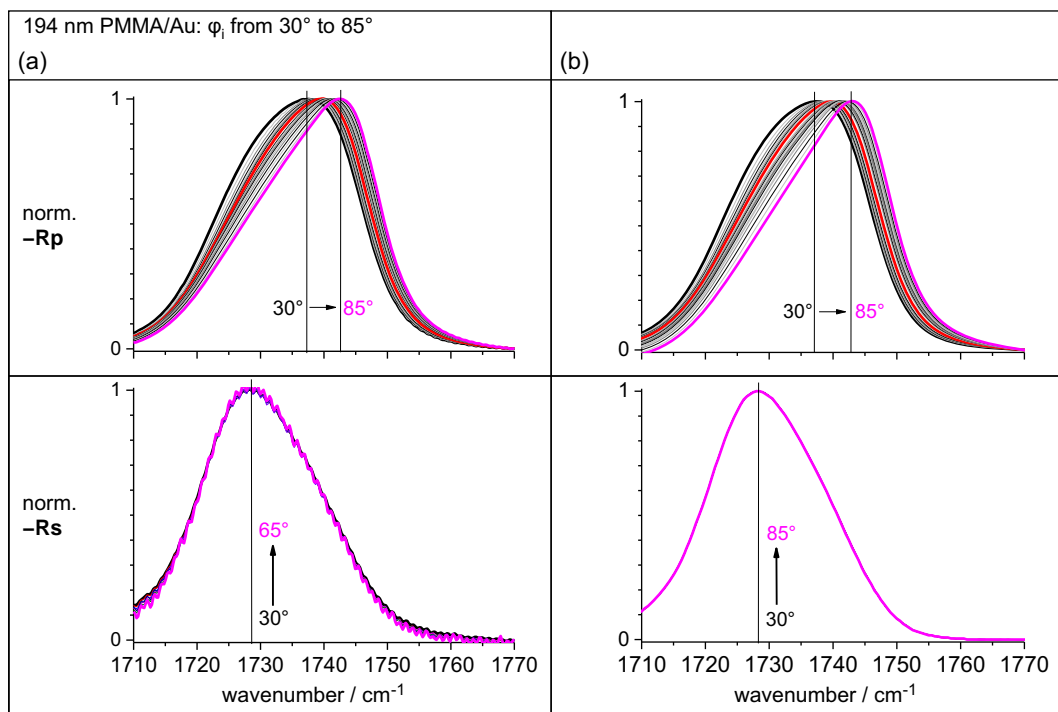


**Figure 6.** Incidence-angle-dependent a) measured and b) calculated normalized p- and s-polarization-dependent negative reflection spectra ($-R_p$ and $-R_s$) of a 194 nm PMMA layer on gold at 0.5 cm$^{-1}$ spectral resolution. To guide the eye, the vertical lines indicate the band maxima at the labeled incidence angles (5° steps till 75°, 1° steps from 75°). Selected spectra are shown as thick lines: 30° (black), 70° (red), and 85° (magenta).

**ADVANCED
SCIENCE NEWS**

www.advancedsciencenews.com

**ADVANCED
PHOTONICS
RESEARCH**

www.adpr-journal.com

**Figure 7.** Incidence-angle-dependent a) measured and b) calculated normalized p- and s-polarization-dependent reflection spectra ($R_p$ and $R_s$) of a 183 nm PMMA layer on silicon at 0.5 cm$^{-1}$ spectral resolution (5° steps till 75°, 1° steps from 76°). Selected spectra are shown as thick lines: 30° (black), 70° (blue), and 85° (magenta).

an overlaid resonance (due to polarizers, see Supporting Information) are identified.

**Figure 8** compares calculated band amplitudes for the s-polarized reflection as expected for the 194 nm PMMA layer on a gold and for the 183 nm PMMA layer on a silicon substrate. Obviously, for the semiconducting substrate a considerable contribution of s-polarized absorption is present even at higher incidence angles. In contrast, this is not the case for the previously studied film on Au substrate where, due to the screening of

the metallic substrate, the s-polarized contributions are significantly reduced at higher incidence angles.

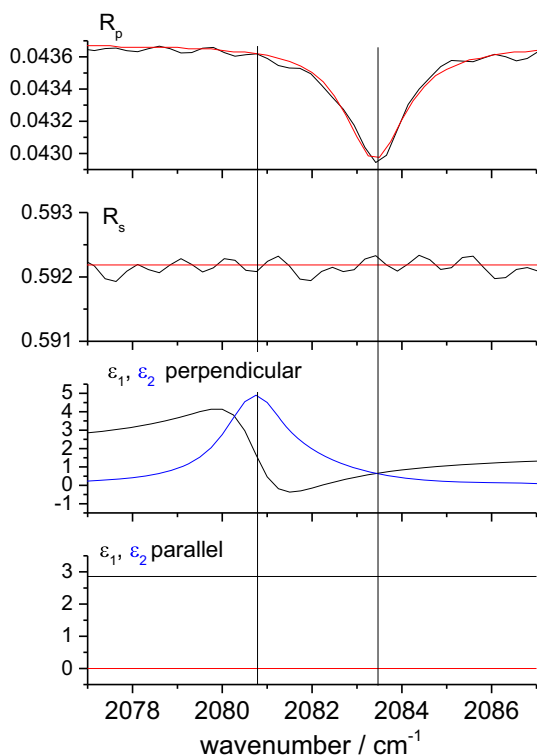### 2.4. Anisotropic Monolayer on Silicon

As a last example, we discuss polarization-dependent IR spectra of an almost perfect anisotropic monolayer sample: the H-passivated Si(111) surface. A particularly noteworthy vibrational band of this surface is the Si–H stretching vibration because it exhibits only a transition dipole moment in direction of the surface normal (z-direction). This allows for studying the frequency shift and shape of a band with strong absorption without a contribution of in-plane-related absorption. This also means that no absorption can occur in s-polarized spectra.

**Figure 9** (top) shows measured (black) and calculated (red) p- and s-polarized reflection spectra ($R_p$ and $R_s$) of a pristine H-passivated Si(111) surface. The observed band at about 2081 cm$^{-1}$ is related to the absorption of the H–Si stretching vibrations. For a best-fit simulation, a thickness of 0.48 nm, an $n_\infty$ of 1.69, and a harmonic oscillator in a uniaxial layer model were assumed.

The results of the best-fit simulation for the direction-dependent complex dielectric function ($\varepsilon_1$ and $\varepsilon_2$) are shown in Figure 9 (bottom). Interestingly, the mode at about 2080.8 cm$^{-1}$ in the dielectric function is shifted strongly toward higher wavenumbers in the measured $R_p$ spectra (2083.4 cm$^{-1}$). It is identified as a so-called Berreman mode.[81,83] This assignment was already discovered decades ago in
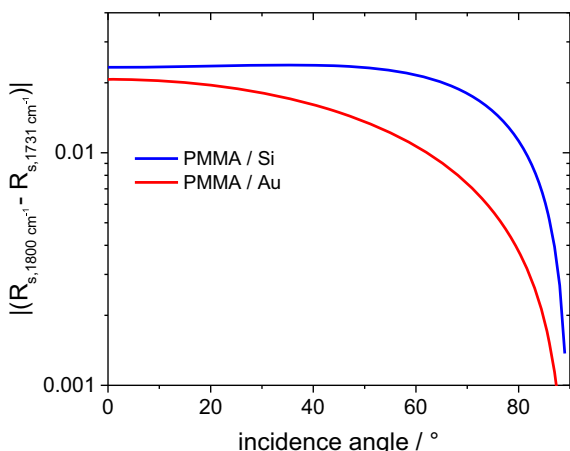


**Figure 8.** s-polarized ($R_s$) band amplitudes ($R_{s,1800\,cm^{-1}} - R_{s,1731\,cm^{-1}}$) of a 194 nm thick PMMA layer on gold and a 183 nm thick PMMA layer on silicon in dependence of the incidence angle.

**ADVANCED
SCIENCE NEWS**

www.advancedsciencenews.com

**ADVANCED
PHOTONICS
RESEARCH**
Open Access

www.adpr-journal.com

**Figure 9.** Top: Measured (black) and simulated (red) p- and s-polarized reflection spectra ($R_p$ and $R_s$) of an H-passivated Si(111) surface (65° incidence angle, 0.5 cm$^{-1}$ spectral resolution). Bottom: Direction-dependent complex dielectric function, with real part $\varepsilon_1$ (black) and imaginary part $\varepsilon_2$ (blue).

ref. [84]. Somehow, this interesting property of H-passivated Si(111) surfaces has fallen into oblivion. It does, however, have interesting consequences for the interpretation of vibrational bands in spectra of such H-passivated surfaces because the Berreman mode is a "macroscopic phenomenon of electrodynamics and not a microscopic problem of molecular dynamics".[85] In other words, despite the fact that such a macroscopic wave is depending on the strengths, orientation, and density of microscopic vibrational resonances (here Si–H stretching vibrations), its excitation is a consequence of the samples geometry and macroscopic dielectric function. Note that only small incidence-angle-dependent shifts are expected for this mode in an ultrathin film.[86]

Such Berreman- and other epsilon-near-zero (ENZ) modes have interesting methodic consequences. For example, resonantly enhanced second harmonic generation (SHG) can be observed from such modes[87] and they can be of advantage for classical IR analysis of ultrathin films and structured surfaces.[88,89] These modes have a broad potential for developments in areas such as for novel platforms for photonic devices,[90,91] including switchable absorbers,[92] optical fibers,[93] compact solid-state attosecond light sources,[94] and optomechanics.[95]

## 3. Concluding Discussion

Several examples for IR spectroscopy of thin isotropic polymer films on different substrates as well as an anisotropic

hydrogen-passivated silicon surface were discussed as case studies for materials with vibrational oscillators from weak to very strong oscillator strengths. For the isotropic polymer films, the band shapes in s-polarized spectra are independent of the incidence angle and are similar to the ones in the imaginary part of the dielectric function. In contrast, strong spectral variations are identified for p-polarized or unpolarized reflection measurements. The band shapes related to strong oscillators are significantly modified at low incidence angles by the spectrally different contribution for in-plane and out-of-plane absorption. In addition, such bands are observed at different frequencies for increasing incidence angles. When studying a film on a semiconducting substrate (here partial screening of the in-plane directed dipole moments), the band shapes of such strong oscillators in p-polarized spectra are substantially modified due to the relatively stronger contribution of in-plane absorption.

In summary, the interpretation of such spectra that probe also out-of-plane absorptions is only possible using optical calculations/simulations. For the 200 nm thick PMMA films on Au and silicon as well as for the hydrogen monolayer on Si(111), the strong influence of the oscillator strengths and incidence angle on the observed band properties in IR spectra of thin films was analyzed. The study of oscillator strengths is useful for multifold analyses, e.g., the oscillator strengths are material specific and their direction dependence can be used for structural analysis. In addition, because the oscillator strength is a direction- and density-dependent property, the observed band properties can also be strongly dependent on the morphology.[96] For a homogeneizable material (the probing wavelength is much larger than any structural unit), varying oscillator densities would also be expected for material mixtures.

To conclude with a comprehensive picture of the situation, the spectral variations in dependence of thickness, incidence angle, and oscillator strength around the respective values of the studied PMMA film are calculated and visualized in **Figure 10**. Figure 10a shows incidence-angle-dependent normalized p-polarized reflection spectra for a constant thickness but with varying oscillator strength. The results demonstrate a concurrent dispersion of the band frequency in dependence of the incidence angle and the oscillator strength. The front plane of the spectra cube corresponds to an assumed strong oscillator ($F = 400$ cm$^{-1}$) which would enable the excitation of a Berreman mode (close to the position of $\varepsilon_1 = 0$, $n = k$ when $n < 1$). For the used $\Gamma = 18.4$ cm$^{-1}$ this situation corresponds to the one of the H-passivated surface. The marked middle plane corresponds to the properties of the studied PMMA film ($F = 208.1$ cm$^{-1}$). The back plane represents an assumed weak oscillator ($F = 50$ cm$^{-1}$), showing a band frequency close to the band position of the resonance frequency. A separate band associated with the in-plane-related absorption becomes apparent at low incidence angles.

Figure 10b visualizes the dispersion in dependence of the incidence angle, but at a fixed oscillator strength. Here, in addition, stronger superposed thickness-dependent influences are observed. Because of a less effective screening of the in-plane polarized absorption at higher thicknesses, the in-plane-related absorption contributes more strongly to the observed band. At low incidence angles (25°, 45°), this leads to decreasing band frequencies with increasing thickness.

Calculated spectral IR bands for a single fixed resonance ($\nu_0$: 1731 cm$^{-1}$; F: 208.1 cm$^{-1}$; $\Gamma$: 18.4 cm$^{-1}$)

(a) PMMA / Au: d= constant = 200 nm

(b) PMMA / Au: F= constant = 208.1 cm$^{-1}$
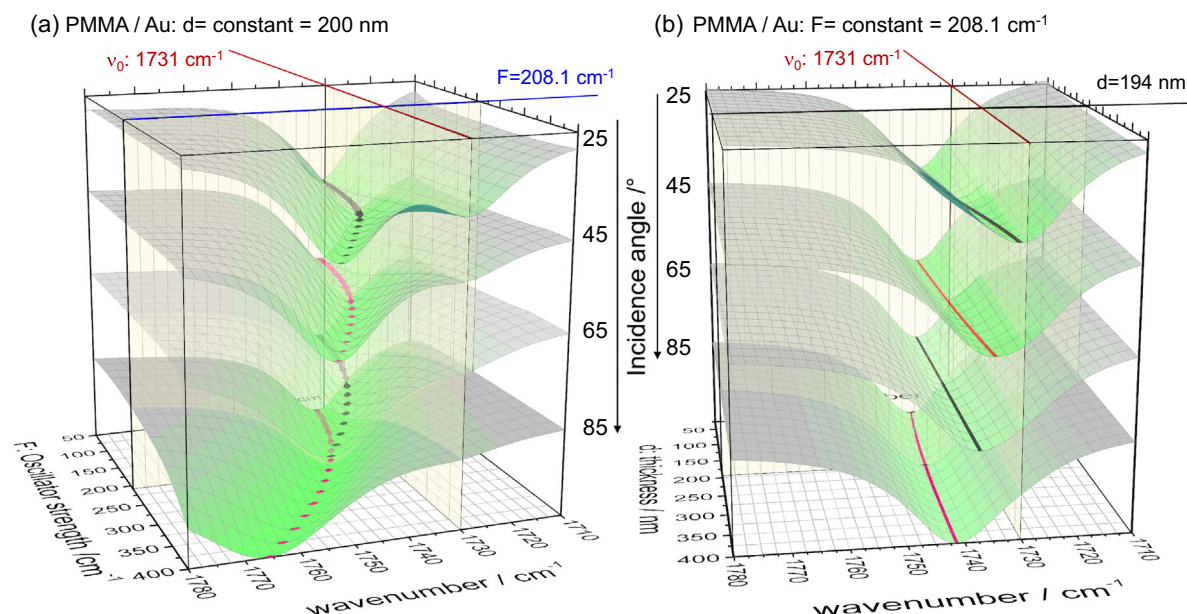


**Figure 10.** Calculated normalized incidence-angle-dependent p-polarized reflection spectra of a PMMA film on Au in dependence of a) oscillator strength and b) thickness. For the calculation, a single Lorentz oscillator (according to Figure S1, Supporting Information) was used to describe PMMA. The plane for the used frequency of the oscillator at 1731 cm$^{-1}$ is marked. Perpendicular to this plane, the other marked planes are a) the oscillator strength of 208.1 cm$^{-1}$ (corresponding to PMMA material properties) and b) the thickness of 194 nm.

In conclusion, the shown manifold dependencies of observed band properties in IR spectra of thin films suggest the necessity of optical interpretations in order to understand the relations of spectra to material properties, thickness, structure, and morphology. On the other hand, optical interpretations also emphasize that IR spectroscopy is a structure sensitive technique suitable for detailed studies of interfaces, thin films, and multilayer samples. We would like to note that related effects can also be present in transmission spectra and are not limited to the IR spectral range.[97]

## Supporting Information

Supporting Information is available from the Wiley Online Library or from the author.

## Conflict of Interest

The authors declare no conflict of interest.

## Data Availability Statement

The data that support the findings of this study are available from the corresponding author upon reasonable request.

[1] V. P. Elanjeitsenni, K. Vadivu, B. M. Prasanth, *Mater. Res. Express* **2022**, *9*, 022001.

[2] A. Bétard, R. A. Fischer, *Chem. Rev.* **2012**, *112*, 1055.

[3] B. Kumar, B. K. Kaushik, Y. S. Negi, *Polym. Rev.* **2014**, *54*, 33.

[4] L. Martin, A. Rappe, *Nat. Rev. Mater.* **2017**, *2*, 16087.

[5] C. E. Ren, K. B. Hatzel, M. Alhabeb, Z. Ling, K. A. Mahmoud, Y. Gogotsi, *J. Phys. Chem. Lett.* **2015**, *6*, 4026.

[6] Z. Yang, P.-F. Sun, X. Li, B. Gan, L. Wang, X. Song, H.-D. Park, C. Y. Tang, *Environ. Sci. Technol.* **2020**, *54*, 15563.

[7] X. Yu, J. Qiu, Q. Hu, K. Chen, J. Zheng, S. Liang, M. Du, H. Ye, *Opt. Express* **2022**, *30*, 43590.

[8] S. Guoab, S. Dong, *Chem. Soc. Rev.* **2011**, *40*, 2644.

[9] T. D. Lee, A. U. Ebong, *Renew. Sustain. Energy Rev.* **2017**, *70*, 1286.

[10] A. D. Franklin, *Science* **2015**, *349*, aab2750.

[11] S. A. DiBenedetto, A. Facchetti, M. A. Ratner, T. J. Marks, *Adv. Mater.* **2009**, *21*, 1407.

[12] M. J. Fasolka, A. M. Mayes, *Annu. Rev. Mater. Res.* **2001**, *31*, 323.

[13] *Ellipsometry of Functional Organic Surfaces and Films*, 2nd ed. (Eds: K. Hinrichs, K.-J. Eichhorn), Springer Series in Surface Sciences, Vol. 52, Springer Nature, Cham **2018**.

[14] R. S. Pedanekar, S. K. Shaikh, K. Y. Rajpure, *Curr. Appl. Phys.* **2020**, *20*, 931.

[15] F. Zaera, *Chem. Soc. Rev.* **2014**, *43*, 7624.

[16] A. M. Monaco, M. Giugliano, *Beilstein J. Nanotechnol.* **2014**, *5*, 1849.

[17] V. K. Vendra, L. Wu, S. Krishnan, in *Nanotechnologies for the Life Sciences* (Ed: C. S. S. R. Kumar), Wiley-VCH, Weinheim **2011**, https://doi.org/10.1002/9783527610419.ntls0179.

[18] S.-J. Lee, D. Asheghali, B. Blevins, R. Timsina, T. Esworthy, X. Zhou, H. Cui, S. Y. Hann, X. Qiu, A. Tokarev, S. Minko, L. G. Zhang, *ACS Appl. Mater. Interfaces* **2020**, *12*, 2067.

[19] L. H. Kidder, A. S. Haka, E. N. Lewis, in *Handbook of Vibrational Spectroscopy* (Eds: J. M. Chalmers, P. R. Griffiths), John Wiley & Sons, Ltd., Hoboken, NJ **2006**.

[20] V. P. Tolstoy, I. Chernyshova, V. A. Skryshevsky, *Handbook of Infrared Spectroscopy of Ultrathin Films*, John Wiley & Sons, Hoboken, NJ **2003**.

[21] A. Dazzi, C. B. Prater, *Chem. Rev.* **2017**, *117*, 5146.

[22] A. Centrone, *Annu. Rev. Analyt. Chem.* **2015**, *8*, 101.

[23] M. Jin, F. Lu, M. Belkin, *Light Sci. Appl.* **2017**, *6*, e17096.

[24] F. S. Ruggeri, C. Byrne, L. Khemtemourian, G. Ducouret, G. Dietler, Y. Jacquot, *J. Pept. Sci.* **2015**, *21*, 95.

[25] C.-M. Pradier, Y. J. Chabal, *Biointerface Characterization by Advanced IR Spectroscopy*, Elsevier B.V., Amsterdam **2011**.

[26] A. A. Govyadinov, I. Amenabar, F. Huth, P. S. Carney, R. Hillenbrand, *J. Phys. Chem. Lett.* **2013**, *4*, 1526.

[27] B. Pollard, E. Muller, K. Hinrichs, M. B. Raschke, *Nat. Commun.* **2014**, *5*, 3587.

[28] N. T. Hunt, *Chem. Soc. Rev.* **2009**, *38*, 1837.

[29] G. Giubertoni, F. Caporaletti, S. J. Roeters, A. S. Chatterley, T. Weidner, P. Laity, C. Holland, S. Woutersen, *Biomacromolecules* **2022**, *23*, 5340.

[30] F. M. Mirabella, in *Handbook of Vibrational Spectroscopy* (Eds: J. M. Chalmers, P. R. Griffiths), John Wiley & Sons, Ltd., Hoboken, NJ **2006**.

[31] D. Allara, J. Stapleton, *Surface Science Techniques, Methods of IR Spectroscopy for Surfaces and Thin Films*, Vol. 51, **2013**, pp. 59–98.

[32] R. W. Hannah, in *Handbook of Vibrational Spectroscopy* (Eds: J. M. Chalmers, P. R. Griffiths), John Wiley & Sons, Ltd, Hoboken, NJ **2006**.

[33] A. Röseler, E. H. Korte, in *Handbook of Vibrational Spectroscopy* (Eds: J. M. Chalmers, P. R. Griffiths), John Wiley & Sons, Ltd., Hoboken, NJ.

[34] K. Hinrichs, A. Furchner, J. Rappich, T. W. H. Oates, *J. Phys. Chem. C* **2013**, *117*, 13557.

[35] A. Furchner, C. Kratz, W. Ogieglo, I. Pinnau, J. Rappich, K. Hinrichs, *J. Vac. Sci. Technol. B* **2020**, *38*, 014003.

[36] A. Furchner, K. Hinrichs, *Adv. Opt. Technol.* **2022**, *11*, 55.

[37] K. Hinrichs, B. Blevins, A. Furchner, N. S. Yadavalli, S. Minko, R. Horvath, M. Mangold, *Nat. Sci.* **2023**, *3*, e20220056.

[38] J. Humlicek, in *Handbook of Ellipsometry* (Eds: H. G. Tompkins, E. A. Irene), William Andrew Publishing, Norwich, NY **2005**, p. 12.

[39] R. M. A. Azzam, N. M. Bashara, *Ellipsometry and Polarized Light*, North Holland Publishing Company, Amsterdam **1977**.

[40] C. Walder, M. Zellmeier, J. Rappich, H. Ketelsen, K. Hinrichs, *Appl. Surf. Sci.* **2017**, *416*, 397.

[41] K. Hinrichs, T. Shaykhutdinov, *Appl. Spectrosc.* **2018**, *72*, 817.

[42] G. E. Jellison, in *Handbook of Ellipsometry* (Eds: H. G. Tompkins, E. A. Irene), William Andrews Publications, Norwich, NY **2005**, p. 282.

[43] P. Yeh, *J. Opt. Soc. Am.* **1979**, *69*, 742.

[44] A. N. Parikh, D. L. Allara, *J. Chem. Phys.* **1992**, *96*, 927.

[45] D. W. Berreman, *J. Opt. Soc. Am.* **1972**, *62*, 502.

[46] M. Schubert, *Phys. Rev. B* **1996**, *53*, 4265.

[47] F. Schreier, *J. Quant. Spectrosc. Radiat. Transfer* **2011**, *112*, 1010.

[48] P. Borowski, S. Pasieczna-Patkowska, M. Barczak, K. Pilorz, *J. Phys. Chem. A* **2012**, *116*, 7424.

[49] G. W. Trucks, K. Raghavachari, G. S. Higashi, Y. J. Chabal, *Phys. Rev. Lett.* **1990**, *65*, 504.

[50] N. Herbots, J. M. Shaw, Q. B. Hurst, M. P. Grams, R. J. Culbertson, D. J. Smith, V. Atluri, P. Zimmerman, K. T. Queeney, *Mater. Sci. Eng. B* **2001**, *87*, 303.

[51] A. Henriksson, P. Neubauer, M. Birkholz, *Adv. Mater. Interfaces* **2021**, *8*, 2100927.

[52] K. Hinrichs, R. Roodenko, J. Rappich, M. M. Chehimi, J. Pinson, in *Analytical Methods for the Characterization of Aryl Layers (Aryl Diazonium Diazonium Salts)* (Eds: M. M. Chehimi), Wiley, Weinheim **2012**.

[53] C. Kratz, A. Furchner, G. Sun, J. Rappich, K. Hinrichs, *J. Phys.: Condens. Matter* **2020**, *32*, 393002.

[54] B. J. Hallam, P.-G. Hamer, A. M. Ciesla née Wenham, C. E. Chan, B. V. Stefani, S. Wenham, *Prog. Photovolt. Res. Appl.* **2020**, *28*, 1217.

[55] S. H. Lee, M. F. Bhopal, D. W. Lee, S. H. Lee, *Mater. Sci. Semicond. Process.* **2018**, *79*, 66.

[56] Y. Shi, M. E. Jones, M. S. Meier, M. Wright, J.-I. Polzin, W. Kwapil, C. Fischer, M. C. Schubert, C. Grovenor, M. Moody, R. S. Bonilla, *Sol. Energy Mater. Sol. Cells* **2022**, *246*, 111915.

[57] P. Jakob, Y. J. Chabal, K. Raghavachari, P. Dumas, S. B. Christman, *Surf. Sci.* **1993**, *285*, 251.

[58] K. Hinrichs, M. Gensch, A. Röseler, N. Esser, *J. Phys.: Condens. Matter* **2004**, *16*, S4335.

[59] I. Zailer, J. E. F. Frost, V. Chabasseur-Molyneux, C. J. B. Ford, M. Pepper, *Semicond. Sci. Technol.* **1996**, *11*, 1235.

[60] Y. Hirai, T. Yoshikawa, N. Takagi, S. Yoshida, K. Yamamoto, *J. Photopolym. Sci. Technol.* **2003**, *16*, 615.

[61] J. Y. Cheng, C. W. Wei, K. H. Hsu, T. H. Young, *Sens. Actuators B: Chem.* **2004**, *99*, 186.

[62] H. Yang, A. Jin, Q. Luo, J. Li, C. Gu, Z. Cui, *Microelectron. Eng.* **2008**, *85*, 814.

[63] K. Koshelev, M. Ali Mohammad, T. Fito, K. L. Westra, S. K. Dew, M. Stepanova, *J. Vac. Sci. Technol. B* **2011**, *29*, 06F306.

[64] U. Ali, K. J. B. A. Karim, N. A. Buang, *Polym. Rev.* **2015**, *55*, 678.

[65] B. Philip, J. K. Abraham, A. Chandrasekhar, *Smart Mater. Struct.* **2003**, *12*, 935.

[66] J. K. Abraham, B. Philip, A. Witchurch, V. K. Varadan, C. C. Reddy, *Smart Mater. Struct.* **2004**, *13*, 1045.

[67] Y. Jin, K. H. Wong, A. M. Granville, *Colloids Surf. A* **2016**, *492*, 100.

[68] S. Gorelick, J. Vila-Comamala, V. Guzenko, R. Mokso, M. Stampanoni, C. David, *Microelectron. Eng.* **2010**, *87*, 1052.

[69] H. Klank, J. P. Kutter, O. Geschke, *Lab Chip* **2002**, *2*, 242.

[70] Y. Xu, W. Wang, Y. Ge, H. Guo, X. Zhang, S. Chen, Y. Deng, Z. Lu, H. Zhang, *Adv. Funct. Mater.* **2017**, *27*, 1.

**ADVANCED
SCIENCE NEWS**

www.advancedsciencenews.com

**ADVANCED
PHOTONICS
RESEARCH**
Open Access

www.adpr-journal.com

[71] G. B. Barin, Y. Song, I. D. F. Gimenez, A. G. S. Filho, L. S. Barreto, J. Kong, *Carbon* **2015**, *84*, 82.

[72] T. Uwanno, Y. Hattori, T. Taniguchi, K. Watanabe, K. Nagashio, *2D Mater.* **2015**, *2*, 041002.

[73] H. He, K. H. Kim, A. Danilov, D. Montemurro, L. Yu, Y. W. Park, F. Lombardi, T. Bauch, K. Moth-Poulsen, T. Iakimov, R. Yakimova, P. Malmberg, C. Müller, S. Kubatkin, S. Lara-Avila, *Nat. Commun.* **2018**, *9*, 3956.

[74] J. Dybal, S. Krimm, *Macromolecules* **1990**, *23*, 1301.

[75] a) F. J. Boerio, S. Wirasate, in *Handbook of Vibrational Spectroscopy* (Eds: J. M. Chalmers, P. R. Griffiths), John Wiley & Sons, Ltd., Hoboken, NJ **2006–2007**, https://doi.org/10.1002/9780470027325.s6104.pub2; b) H. W. Siesler, G. G. Hoffmann, O. Kolomiets, F. Pfeifer, M. Zahedi, in *Handbook of Vibrational Spectroscopy* (Eds: J. M. Chalmers, P. R. Griffiths), John Wiley & Sons, Ltd., Hoboken, NJ **2006–2007**, https://doi.org/10.1002/9780470027325.s6201.pub2.

[76] J. Spévácek, B. Schneider, J. Dybal, J. Stokr, *J. Croat. Chem. Acta* **1987**, *60*, 11.

[77] S. Tsuda, S. Yamaguchi, Y. Kanamori, H. Yugami, *Opt. Express* **2018**, *26*, 6899.

[78] R. G. Greenler, D. R. Snider, D. Witt, R. S. Sorbello, *Surf. Sci.* **1982**, *118*, 415.

[79] E. Bortchagovsky, T. Mishakova, *Appl. Opt.* **2023**, *62*, 904.

[80] K. Hinrichs, J. Rappich, T. Shaykhutdinov, *Phys. Status Solidi B* **2020**, *257*, 2070022.

[81] D. W. Berreman, *Phys. Rev.* **1963**, *130*, 2193.

[82] B. Xiang, W. Xiong, *J. Chem. Phys.* **2021**, *155*, 050901.

[83] A. Röseler, in *Handbook of Ellipsometry* (Eds: H. G. Tompkins, E. A. Irene), William Andrew Publishing, Norwich, NY **2005**, pp. 763–798.

[84] W. Henrion, A. Roeseler, H. Angermann, M. Rebien, *Phys. Status Solidi A* **1999**, *175*, 121.

[85] P. Grosse, V. Offermann, *Vib. Spectrosc.* **1995**, *8*, 121.

[86] S. Vassant, J.-P. Hugonin, F. Marquier, J.-J. Greffet, *Opt. Express* **2012**, *20*, 23971.

[87] N. C. Passler, I. Razdolski, D. S. Katzer, D. F. Storm, J. D. Caldwell, M. Wolf, A. Paarmann, *ACS Photonics* **2019**, *6*, 1365.

[88] T. Shaykhutdinov, A. Furchner, J. Rappich, K. Hinrichs, *Opt. Mater. Express* **2017**, *7*, 3706.

[89] J.-Th. Zettler, M. Weidner, A. Röseler, *Phys. Status Solidi A* **1991**, *124*, 547.

[90] J. Wu, Z. T. Xie, Y. Sha, H. Y. Fu, Q. Li, *Photon. Res.* **2021**, *9*, 1616.

[91] X. Niu, X. Hu, S. Chu, Q. Gong, *Adv. Opt. Mater.* **2018**, *6*, 1701292.

[92] Z. Wang, P. Zhou, G. Zheng, *Results Phys.* **2019**, *14*, 102376.

[93] J. Yang, K. Minn, A. Anopchenko, S. Gurung, H. W. H. Lee, *Laser Photonics Rev.* **2023**, *17*, 2200539.

[94] Y. Yang, J. Lu, A. Manjavacas, T. S. Luk, H. Liu, K. Kelley, J.-P. Maria, E. L. Runnerstrom, M. B. Sinclair, S. Ghimire, I. Brener, *Nat. Phys.* **2019**, *15*, 1022.

[95] Y. Kiasat, M. G. Donato, M. Hinczewski, M. M. Elkabbash, T. Letsou, R. Sajia, O. M. Marago, G. Strangi, N. Engheta, *Commun. Phys.* **2023**, *6*, 69.

[96] N. Nagai, H. Okada, T. Hasegawa, *AIP Adv.* **2019**, *9*, 105203.

[97] E. G. Bortchagovsky, U. C. Fischer, *J. Chem. Phys.* **2002**, *117*, 5384.